

# Controlling biological networks by time-delayed signals

BY GÁBOR OROSZ<sup>1,\*</sup>, JEFF MOEHLIS<sup>1</sup> AND RICHARD M. MURRAY<sup>2</sup>

<sup>1</sup>*Department of Mechanical Engineering, University of California,  
Santa Barbara, CA 93106, USA*

<sup>2</sup>*Control and Dynamical Systems, California Institute of Technology,  
Pasadena, CA 91125, USA*

This paper describes the use of time-delayed feedback to regulate the behaviour of biological networks. The general ideas on specific transcriptional regulatory and neural networks are demonstrated. It is shown that robust yet tunable controllers can be constructed that provide the biological systems with model-engineered inputs. The results indicate that time delay modulation may serve as an efficient biocompatible control tool.

**Keywords:** time delay; control; gene regulatory network; neural network

## 1. Introduction

A common rule of thumb in engineering is that time delays can cause undesired oscillations. For example, the use of high-frequency digital controllers (which introduce tiny delays into the control loops) can result in low-frequency vibrations in robotic systems (Stépan 2001). In most cases, engineers are able to overcome these problems by using predictor algorithms (Mascolo 1999). It may also be the case that vibrations disappear for windows of larger delay where the efficiency of technological processes can even be higher (Dombovári *et al.* 2008).

Recent papers have demonstrated that time delays can play important roles in biological systems. For example, in gene-regulatory networks, oscillations in protein levels may arise due to time delays (Monk 2003; Novák & Tyson 2008), and existing oscillations may become more robust (Stricker *et al.* 2008; Ugander 2008). Similarly, in neural networks, delays may initiate different rhythmic spatiotemporal patterns (Coombes & Laing 2009) and alter the stability of existing patterns (Ermentrout & Ko 2009). Some authors suggest that neural systems may even exploit time delays when encoding information into spatiotemporal codes (Kirst *et al.* 2009; Orosz *et al.* 2009*a*).

New interfaces allow us to interact with biological networks, i.e. to sense and regulate their behaviour (Chalfie *et al.* 1994; Popovych *et al.* 2006; Sarpeshkar *et al.* 2008). To design such regulators, one needs to use techniques from control and dynamical systems theory (Åström & Murray 2008). In this paper, we demonstrate that tuning the time delays may provide us with additional ‘degrees

\*Author for correspondence (gabor@engineering.ucsb.edu).

One contribution of 13 to a Theme Issue ‘Delayed complex systems’.

of freedom' for suppressing or changing the rhythmic behaviour in biological systems. Broadly speaking, besides varying the strength of the control actions (i.e. the gains), one may also modulate the timing of the actions by varying the delays. Such a strategy is usually avoided in engineering systems since it requires the use of delay differential equations and infinite-dimensional state spaces. On the other hand, exploiting the richness of such dynamics may prove to be beneficial when interacting with living organisms.

We demonstrate these ideas in two different biological networks. In §2, we consider a simple synthetic gene regulatory circuit, called the repressilator. We show that one may stabilize the steady state of protein expression by using an additional regulatory gene with appropriate time delays. In §3, a simple neural network is studied. Based on the stability analysis of oscillatory solutions, we construct an event-based act-and-wait type of controller that uses delayed inputs to drive the system into a chosen oscillatory state. Finally, in §4, we conclude and discuss future research directions.

## 2. Controlling equilibria in gene regulatory networks

Intracellular spaces are filled with biochemical regulatory networks in every organism. In particular, gene regulatory networks allow cells to express proteins when needed (Bolouri 2008; Courey 2008). Genes (sections of DNA) are transcribed into mRNA (by RNA polymerase) and then mRNA is translated into proteins (by ribosomes). The resulting proteins go through configurational changes (called folding) to become 'biochemically active'. An active protein then may bind to the so-called promoter region of another gene and activate or repress the transcription of the gene (and in turn regulate the expression of the corresponding protein). Indeed, both transcription and translation takes a finite amount of time, which introduces time delays into the modelling equations (Monk 2003; Novák & Tyson 2008).

Owing to the large number of genes in living cells, it is very difficult to map out the dynamics of natural gene regulatory networks. For this reason, a different approach was initiated about a decade ago when the first synthetic transcriptional regulatory circuits were constructed and implanted into living cells (see Elowitz & Leibler (2000) for the repressilator and Gardner *et al.* (2000) for the toggle switch). Using fluorescent proteins as output signals, the dynamics of synthetic circuits can be studied in detail (Chalfie *et al.* 1994).

Gene regulatory networks can exhibit robust oscillatory behaviour. For example, circadian rhythms in cells are driven by such genetic oscillations (Dunlap 1999). On the other hand, mutant genes may lead to pathological oscillations (Novák & Tyson 2008). One way to suppress such oscillations might be to implant extra regulatory genes into the cells. One can design where to 'take a signal out' by implanting a gene that is repressed or activated by a chosen protein of the system. It is also possible to 'insert a signal' by using a protein that activates or represses a chosen gene in the system. However, to stabilize an equilibrium without changing it (i.e. without changing the steady-state values of mRNA and protein concentrations), the gains need to satisfy extra constraints. These constraints may still allow stabilization if additional time delays are built into the controller. Note that transcriptional delays may be increased by inserting 'junk'

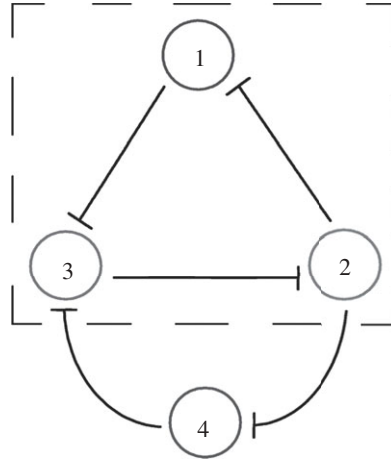


Figure 1. Sketch of the repressilator (subnetwork marked by the dashed frame) with an additional regulatory gene attached.

sections into the gene, and translational delays can be enlarged by slowing down the protein folding (see Ugander (2008) for more details on delay engineering in transcriptional regulatory networks).

Here, we test these ideas on the repressilator, which consists of three genes coupled to each other to form a unidirectional ring as depicted by the subnetwork within the dashed frame in figure 1. Each circle represents a gene and its protein product (Elowitz & Leibler 2000). This circuit shows robust oscillatory behaviour in wide regions of parameters. It was shown that increasing the transcriptional and translational delays between the repressilator elements 1, 2 and 3 leads to more robust oscillations, i.e. they appear in more extended parameter domains and become more attractive (Chen & Aihara 2002; Ugander 2008). On the other hand, we will show that the oscillations can be suppressed by attaching an additional element and choosing the corresponding delays appropriately (see the extra regulatory element 4 outside the dashed frame in figure 1).

The regulated system can be modelled by the delay differential equations

$$\left. \begin{aligned} \dot{m}_i(t) &= -m_i(t) + \alpha f(p_{i+1}(t)), & \dot{p}_i(t) &= -\beta p_i(t) + \beta m_i(t), & i &= 1, 2, \\ \dot{m}_3(t) &= -m_3(t) + \alpha f((1 - \eta)p_1(t) + \eta p_4(t)), & \dot{p}_3(t) &= -\beta p_3(t) + \beta m_3(t), \\ \text{and } \dot{m}_4(t) &= -m_4(t) + \alpha f(p_2(t - \sigma)), & \dot{p}_4(t) &= -\beta p_4(t) + \beta m_4(t - \tau), \end{aligned} \right\} \quad (2.1)$$

where each gene is repressed through the nonlinear function

$$f(p) = \frac{1}{1 + p^n} + f_0, \quad (2.2)$$

which is depicted by the decreasing curve in figure 2. Here the overdot represents the derivative with respect to time  $t$  and  $m_i, p_i \geq 0$  are the concentrations of mRNA and protein for the  $i$ th species. For the sake of simplicity, parameters are chosen to be identical for each gene–protein pair. We assume that the time delays are small in the original system (these are set to zero for  $i = 1, 2, 3$ ), but the extra regulatory element contains significant transcriptional and translational

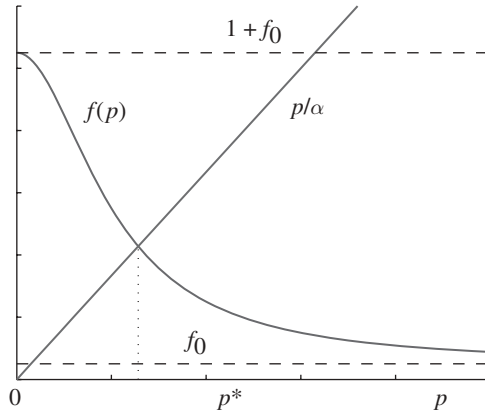


Figure 2. Finding the equilibrium value  $p^*$  of protein concentration. The increasing straight line and the decreasing curve correspond to the left and right sides of the algebraic equation (2.4), in which  $f$  is given by equation (2.2).

delays (denoted by  $\sigma$  and  $\tau$ , respectively). The time is measured in units of mRNA degradation time, the protein concentrations are rescaled by the number of proteins needed to half-maximally repress a gene and the mRNA concentrations are rescaled by the number of proteins expressed per mRNA molecule in steady state. The rescaled parameters  $\alpha$  and  $\beta$  represent the strength of the repression and the protein degradation rate, respectively, and these can be determined from dimensional parameters. In this paper, we consider the ‘leakage constant’  $f_0 = 10^{-3}$  and the Hill coefficient  $n = 2$ , for which oscillations appear in a wide ranges of parameters  $\alpha$  and  $\beta$ . We recall that  $\alpha = 215.52$  and  $\beta = 0.2069$  were used in Elowitz & Leibler (2000), in which oscillations were demonstrated experimentally.

We assume that there is only one binding site at the promoter region of a gene, i.e. in the case of gene 3 either protein  $p_1$  or protein  $p_4$  binds but not both (see figure 1). More precisely, we assume that  $p_4$  binds with probability  $\eta \in [0, 1]$  and so  $p_1$  binds with probability  $(1 - \eta)$ , as expressed in the last term of the equation for  $\dot{m}_3$  in equation (2.1). Notice that, when choosing  $\eta = 0$ , the repressilator with genes 1, 2 and 3 is obtained, while for  $\eta = 1$  another repressilator emerges with genes 2, 3 and 4 and time delays  $\sigma$  and  $\tau$ . In both these special cases, the equilibria are unstable and oscillations occur. As will be shown below, these oscillations may be suppressed for certain intermediate values of  $\eta$  by choosing the delays appropriately. We note that one may model competitive binding by using the nonlinear combination  $\eta_1 f(p_1(t)) + \eta_4 f(p_4(t))$  with  $\eta_1, \eta_4 \geq 0$  instead of  $f((1 - \eta)p_1(t) + \eta p_4(t))$  in the equation for  $\dot{m}_3$  in equation (2.1). The linear stability diagrams obtained in this case are qualitatively similar to those presented in this paper. We also remark that there exist genes with multiple binding sites and one may use the resulting combinatorial features when designing genetic controllers (Cox et al. 2007).

System (2.1) possesses the ‘symmetric’ equilibrium

$$m_i(t) \equiv p_i(t) \equiv p^*, \tag{2.3}$$

for  $i = 1, 2, 3, 4$ , where  $p^*$  is the unique solution of

$$\frac{p}{\alpha} = f(p), \tag{2.4}$$

as demonstrated in figure 2. Note that  $p^* = p^*(\alpha, f_0, n)$  and this is monotonically increasing in  $\alpha$ . Also notice that equation (2.4) is independent of  $\eta, \sigma$  and  $\tau$ , i.e. the extra regulatory gene does not change the equilibrium of the repressilator. This occurs since the parameters  $\alpha$  and  $\beta$  for the extra element 4 are considered to be identical to the parameters for the original system 1, 2 and 3. Modulating these parameters (in the last two equations in equation (2.1) only) may suppress the oscillations but it destroys the symmetry and so changes the equilibrium. Contrarily, varying  $\eta, \sigma$  and  $\tau$  may allow us to stabilize the equilibrium without altering it.

Let us define the perturbations

$$\left. \begin{aligned} a_i(t) &:= m_i(t) - p^* \\ b_i(t) &:= p_i(t) - p^* \end{aligned} \right\} \tag{2.5}$$

and

and introduce the vector notation

$$\left. \begin{aligned} \mathbf{a} &= [a_1 \quad a_2 \quad a_3 \quad a_4]^T \\ \mathbf{b} &= [b_1 \quad b_2 \quad b_3 \quad b_4]^T \end{aligned} \right\} \tag{2.6}$$

and

Thus, the linearization of equation (2.1) about equation (2.3) can be written as

$$\begin{bmatrix} \dot{\mathbf{a}}(t) \\ \dot{\mathbf{b}}(t) \end{bmatrix} = \begin{bmatrix} -\mathbf{I} & \alpha\kappa\mathbf{A}_0 \\ \beta\mathbf{B}_0 & -\beta\mathbf{I} \end{bmatrix} \begin{bmatrix} \mathbf{a}(t) \\ \mathbf{b}(t) \end{bmatrix} + \begin{bmatrix} \mathbf{O} & \alpha\kappa\mathbf{A}_\sigma \\ \mathbf{O} & \mathbf{O} \end{bmatrix} \begin{bmatrix} \mathbf{a}(t-\sigma) \\ \mathbf{b}(t-\sigma) \end{bmatrix} + \begin{bmatrix} \mathbf{O} & \mathbf{O} \\ \beta\mathbf{B}_\tau & \mathbf{O} \end{bmatrix} \begin{bmatrix} \mathbf{a}(t-\tau) \\ \mathbf{b}(t-\tau) \end{bmatrix}, \tag{2.7}$$

where

$$\left. \begin{aligned} \mathbf{A}_0 &= \begin{bmatrix} 0 & 1 & 0 & 0 \\ 0 & 0 & 1 & 0 \\ 1 - \eta & 0 & 0 & \eta \\ 0 & 0 & 0 & 0 \end{bmatrix}, & \mathbf{A}_\sigma &= \begin{bmatrix} 0 & 0 & 0 & 0 \\ 0 & 0 & 0 & 0 \\ 0 & 0 & 0 & 0 \\ 0 & 1 & 0 & 0 \end{bmatrix} \\ \mathbf{B}_0 &= \begin{bmatrix} 1 & 0 & 0 & 0 \\ 0 & 1 & 0 & 0 \\ 0 & 0 & 1 & 0 \\ 0 & 0 & 0 & 0 \end{bmatrix}, & \mathbf{B}_\tau &= \begin{bmatrix} 0 & 0 & 0 & 0 \\ 0 & 0 & 0 & 0 \\ 0 & 0 & 0 & 0 \\ 0 & 0 & 0 & 1 \end{bmatrix} \end{aligned} \right\} \tag{2.8}$$

and

$\mathbf{I}$  and  $\mathbf{O}$  denote the  $4 \times 4$  identity and zero matrices, respectively, and

$$\kappa = f'(p^*) < 0. \tag{2.9}$$

Note that  $p^* = p^*(\alpha, f_0, n)$  implies  $\kappa = \kappa(\alpha, f_0, n)$ .

Now considering the trial solution  $\mathbf{a}(t) = \bar{\mathbf{a}} e^{\lambda t}$  and  $\mathbf{b}(t) = \bar{\mathbf{b}} e^{\lambda t}$  with constant vectors  $\bar{\mathbf{a}}, \bar{\mathbf{b}} \in \mathbb{R}^4$  and eigenvalues  $\lambda \in \mathbb{C}$ , the characteristic equation

$$\begin{aligned} D(\lambda) &= \det \begin{bmatrix} (\lambda + 1)\mathbf{I} & -\alpha\kappa(\mathbf{A}_0 + \mathbf{A}_\sigma e^{-\lambda\sigma}) \\ -\beta(\mathbf{B}_0 + \mathbf{B}_\tau e^{-\lambda\tau}) & (\lambda + \beta)\mathbf{I} \end{bmatrix} \\ &= (\lambda + 1)(\lambda + \beta)\{(\lambda + 1)^3(\lambda + \beta)^3 - (\alpha\beta\kappa)^3(1 - \eta + \eta e^{-\lambda(\sigma+\tau)})\} = 0 \end{aligned} \tag{2.10}$$

is obtained. This equation has infinitely many solutions for the eigenvalues  $\lambda$  in correspondence to the infinite-dimensional state spaces of equations (2.1) and (2.7). The equilibrium (2.3) is asymptotically stable if and only if all eigenvalues lie in the left-half complex plane. When varying the parameters, the equilibrium may lose its stability via Hopf bifurcation if a pair of complex conjugate eigenvalues crosses the imaginary axis. This bifurcation results in

periodic oscillations. To determine the stability boundaries, we substitute  $\lambda = i\omega$ ,  $\omega \in \mathbb{R}^+$  into equation (2.10), separate the real and imaginary parts and apply some trigonometric identities. The stability curves in the  $(\sigma + \tau, \eta)$  parametric plane are given by

$$\sigma + \tau = \frac{1}{\omega} \left\{ \pm \arccos \left( \frac{c_1^2 - c_2^2 - 2c_1 + 1}{c_1^2 + c_2^2 - 2c_1 + 1} \right) + (2\ell + 1)\pi \right\}, \quad \ell = 0, 1, 2, \dots$$

and

$$\eta = \frac{c_1^2 + c_2^2 - 2c_1 + 1}{-2c_1 + 2},$$

(2.11)

where

$$c_1 = \frac{(\beta - \omega^2)((\beta - \omega^2)^2 - 3(1 + \beta)^2\omega^2)}{(\alpha\beta\kappa)^3}$$

and

$$c_2 = \frac{(1 + \beta)\omega(3(\beta - \omega^2)^2 - (1 + \beta)^2\omega^2)}{(\alpha\beta\kappa)^3},$$

(2.12)

and the + and - signs are considered when  $\sin(\omega(\sigma + \tau)) < 0$  and  $\sin(\omega(\sigma + \tau)) > 0$ , respectively.

The curves for  $\ell = 0$  are plotted in figure 3 for different values of  $\alpha$  and  $\beta$ ; the original repressilator parameters are used in figure 3*a*. The curves for  $\ell > 0$  appear for larger delays to the right of the  $\ell = 0$  curves and these are out of the window. Using infinite-dimensional generalizations of the Routh–Hurwitz criteria (Stépán 1989), one may determine that the steady state is linearly stable in the shaded domain. Notice that, when decreasing or increasing  $\alpha$  (figure 3*a–c*), the stable regime does not change significantly, only becoming a bit more extended corresponding to the fact that oscillations appear to be most robust for intermediate values of  $\alpha$  in the uncontrolled repressilator (Elowitz & Leibler 2000). On the other hand, the stable domain shrinks and moves closer to the vertical axis when decreasing  $\beta$  (figure 3*a, d, e*).

When a stability curve crosses itself, a co-dimension-2 Hopf bifurcation occurs, i.e. two pairs of complex conjugate eigenvalues cross the imaginary axis, leading to quasi-periodic oscillations. We remark that such bifurcations occur rarely in dynamical systems without delay but they are quite typical in delayed systems (Stépán 1989). Note that the equilibrium may lose its stability via a steady-state bifurcation when a real eigenvalue crosses the imaginary axis due to parameter variations. This cannot occur here for any  $\sigma, \tau \geq 0$  since  $\kappa = f'(p^*) < 0$ , as can be seen by substituting  $\lambda = 0$  into equation (2.10). We also remark that, incorporating the time delays in the interactions between the repressilator genes 1, 2 and 3, the stability regimes can still be determined; however, the calculations become more elaborate and so less instructive.

In figure 3*a*, we marked the points A and B, and the corresponding numerical simulation results are shown in figure 4*a, b*, respectively. In both cases, the same initial conditions are chosen. Recall that the initial conditions for delay differential equations are functions in the delay interval  $t \in [-\max\{\sigma, \tau\}, 0]$ , which are chosen to be constant functions here. When the equilibrium is unstable (point A in figure 3*a* at  $\sigma + \tau = 15, \eta = 0$ ), oscillations arise. The time profiles for the repressilator protein concentrations  $p_1, p_2$  and  $p_3$  are displayed in the top panel of figure 4*a*. The system approaches a travelling wave solution where the time profile of the  $(i + 1)$ st protein can be obtained by shifting the time profile of

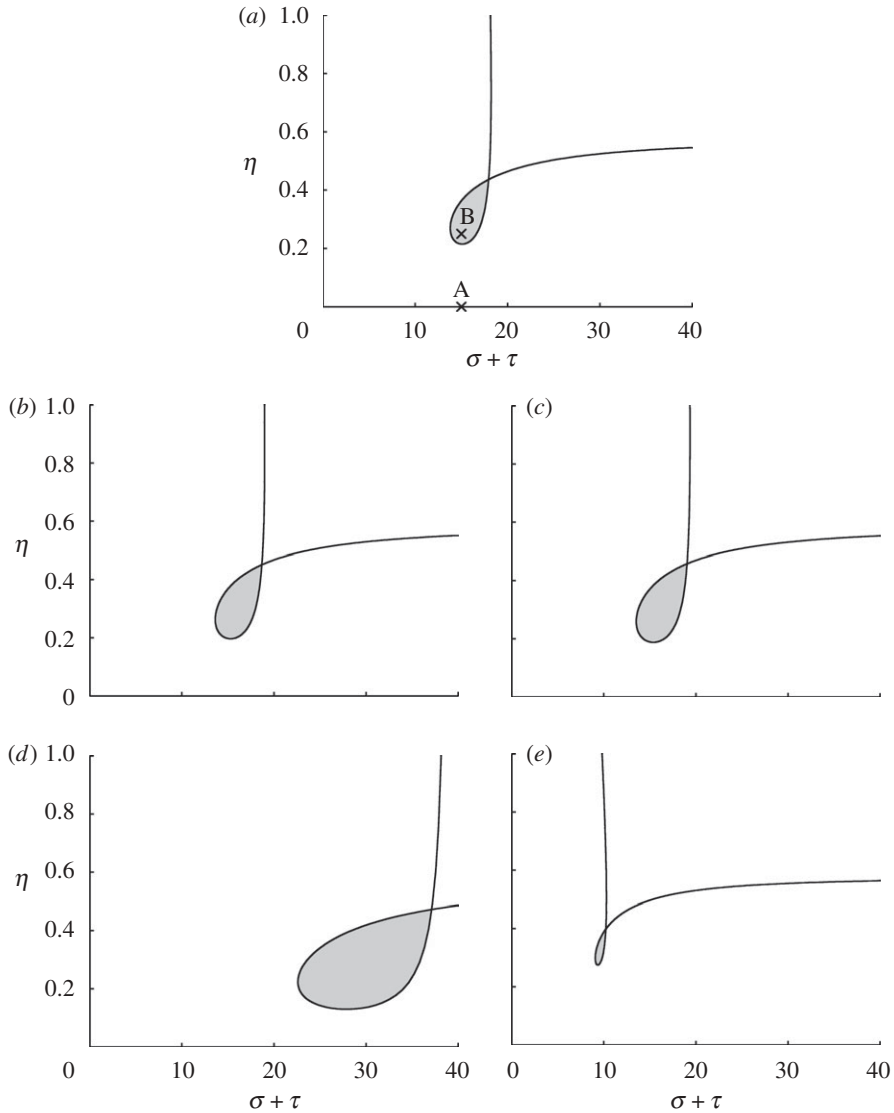


Figure 3. Stability diagrams for the controlled repressilator for different repression strengths  $\alpha$  and protein degradation rates  $\beta$ . The equilibrium (2.3) is linearly stable in the shaded domains. Points A and B in (a) correspond to the simulations shown in figure 4a,b, respectively. (a)  $\alpha = 215.52$ ,  $\beta = 0.2069$ ; (b)  $\alpha = 50$ ,  $\beta = 0.2069$ ; (c)  $\alpha = 800$ ,  $\beta = 0.2069$ ; (d)  $\alpha = 215.52$ ,  $\beta = 0.1$ ; (e)  $\alpha = 215.52$ ,  $\beta = 0.4$ .

the  $i$ th protein by  $T_p/3$ , where  $T_p$  is the period of oscillations. This pattern corresponds to the  $Z_3$  discrete rotational symmetry in the system and may also be interpreted as a splay state, meaning that the concentration of each protein ‘fires’ separately and equidistantly in time. The time evolution for the protein concentration  $p_4$  is shown in the bottom panel in figure 4a. Since  $\eta = 0$  and  $p_1$  and  $p_4$  are both driven by  $p_2$ , the time profiles for  $p_4$  can be obtained by shifting the  $p_1$  signal with  $\sigma + \tau$ . When the equilibrium is stable (point B in

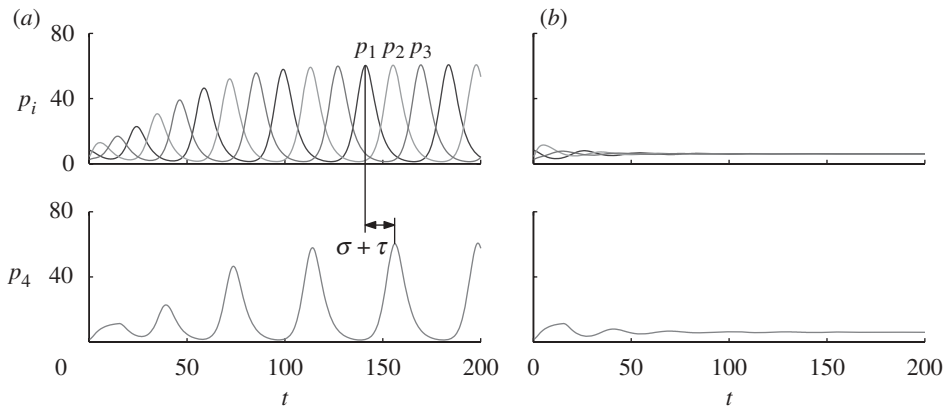


Figure 4. Demonstrating the action of the genetic controller by numerical simulations. The protein concentrations  $p_1$ ,  $p_2$  and  $p_3$  for the repressilator are shown on the top and the protein concentration  $p_4$  for the extra regulatory gene is displayed at the bottom. Panels (a) and (b) correspond to the points A and B in figure 3a.

figure 3a at  $\sigma + \tau = 15$ ,  $\eta = 0.25$ ), no oscillations develop, as shown in figure 4b. This demonstrates that the equilibrium can be stabilized by tuning the aggregated delay  $\sigma + \tau$  and the binding probability  $\eta$ .

We note that one may find oscillations even for a stable equilibrium when considering certain specific initial conditions. This suggests that the Hopf bifurcations may be subcritical. It may be an interesting future research topic to map out the bifurcation structure for the arising periodic solutions, but that is beyond the scope of this paper. In the following section, however, we investigate a time-delayed network where it is essential to study the stability of oscillatory solutions. Such investigations allow us to construct a controller that can stabilize a chosen rhythm.

### 3. Controlling periodic solutions in neural networks

Oscillations are ubiquitous in neural networks: rhythmic patterns of electric activity are used to represent information about the environment and about the state of the animal in many different ways (Rabinovich *et al.* 2006). However, some of these rhythms, e.g. full synchrony, may be pathological and lead to macroscopic tremors such as in Parkinson's disease. (In contrast, in technological systems full synchrony is often desired (Olfati-Saber & Murray 2004).)

One way to avoid these harmful oscillations (without destroying all rhythms) might be to inject weak external current into specific brain areas. For example, when injecting different signals at multiple sites, neurons may entrain their rhythms to the signal of the nearby electrode and so the overall synchrony can be destroyed (Popovych *et al.* 2006). However, this control strategy may force the neural system into an 'artificial state'. Instead, one may select a natural rhythm and try to stabilize it. Since neurons communicate with electric signals (called spikes), it takes a considerable amount of time to transmit the signal from one neuron to another. Consequently, time delays appear in the modelling equations.



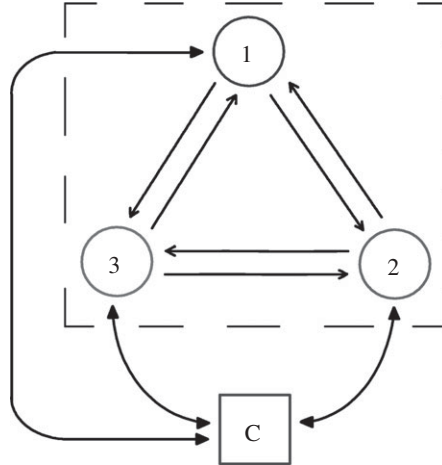


Figure 5. Sketch of a network of three globally coupled neurons (subnetwork marked by the dashed frame) with a controller attached.

When varying the delays, different stable patterns (e.g. full synchrony, clustering) can emerge (Ermentrout & Ko 2009). As will be shown below, one may construct a controller that mimics the delayed interactions of neurons and so drives the system away from synchrony into a chosen cluster state.

We demonstrate these ideas in a simple system of three neurons with all-to-all coupling as depicted inside the dashed frame in figure 5. We assume that the voltage of each neuron can be measured and current can be injected into each cell (see the controller C outside the dashed frame in figure 5). To describe the activity of the neurons, we use the Hodgkin–Huxley model that models the cell membrane as a simple electric circuit (Hodgkin & Huxley 1952). We consider direct electrotonic coupling (gap junctions) between the neurons and incorporate axonal delays to model the time required to transmit the signal along the axons. For simplicity, we omit dendritic delays (associated with signal transmission along dendrites) and synaptic delays (the time needed to release chemicals in synapses); see Campbell (2007) and Ermentrout & Ko (2009) for more details on these effects.

The time evolution of the controlled system is given by the delay differential equations

$$\left. \begin{aligned}
 \dot{V}_i(t) &= \frac{1}{C} \left( I - g_{\text{Na}} m_i^3(t) h_i(t) (V_i(t) - V_{\text{Na}}) \right. \\
 &\quad \left. - g_{\text{K}} n_i^4(t) (V_i(t) - V_{\text{K}}) - g_{\text{L}} (V_i(t) - V_{\text{L}}) \right. \\
 &\quad \left. + \varepsilon \sum_{j=1, j \neq i}^3 (V_j(t - \xi) - V_i(t)) + \delta u_i(t) \right), \\
 \dot{m}_i(t) &= \alpha_m (V_i(t)) (1 - m_i(t)) - \beta_m (V_i(t)) m_i(t), \\
 \dot{h}_i(t) &= \alpha_h (V_i(t)) (1 - h_i(t)) - \beta_h (V_i(t)) h_i(t), \\
 \text{and } \dot{n}_i(t) &= \alpha_n (V_i(t)) (1 - n_i(t)) - \beta_n (V_i(t)) n_i(t), \quad i = 1, 2, 3,
 \end{aligned} \right\} \quad (3.1)$$

where the overdot represents the derivative with respect to time  $t$  (measured in ms),  $V_i$  is the voltage of the  $i$ th neuron (measured in mV) and the dimensionless quantities  $m_i, h_i, n_i \in [0, 1]$  (called gating variables) characterize the ‘openness’ of the sodium and potassium ion channels embedded in the cell membrane. The conductances  $g_{\text{Na}}, g_{\text{K}}$  and  $g_{\text{L}}$  and the reference voltages  $V_{\text{Na}}, V_{\text{K}}$  and  $V_{\text{L}}$  for the sodium channels, potassium channels and the so-called ‘leakage current’ are, respectively, given together with the membrane capacitance  $C$  and the driving current  $I$  in equation (A 1).

The term proportional to  $\varepsilon$  describes the electrotonic coupling between neurons. The conductance  $\varepsilon$  represents the coupling strength and  $\xi$  is the transmission delay described above. The term proportional to  $\delta$  represents the control signal. The coefficient  $\delta$  is the magnitude of the injected current and  $u_i(t)$  describes the time variation of the input and can take the discrete values 0, 1 and 2. We assume that the coupling is weak, i.e.  $\varepsilon \ll 1$ , and that the influence of input is commensurable with the influence of coupling, i.e.  $\delta = \mathcal{O}(|V|\varepsilon)$ . For the parameters considered, we have  $|V| \approx 100$  and here we set  $\delta = 250\varepsilon$ . The equations for  $m_i, h_i$  and  $n_i$  are based on measurements and the nonlinear functions  $\alpha_m(V), \alpha_h(V), \alpha_n(V), \beta_m(V), \beta_h(V)$  and  $\beta_n(V)$  are given in equation (A 2).

First, we describe the dynamics without inputs ( $\delta = 0$ ) when varying the coupling strength  $\varepsilon$  and the coupling delay  $\xi$ . For  $\varepsilon = 0$ , the neurons are uncoupled and spike periodically (with period  $T_p \approx 10.43$ ). For small  $\varepsilon > 0$ , the qualitative shape of oscillations does not change but different cluster states can arise through the interactions. In particular, three different patterns may exist: full synchrony (when all three neurons spike together), splay state (when no neurons spike together) and 1:2 state (when only two neurons spike together). These patterns correspond to the  $S_3$  permutational symmetry in the system (interchangeability of neurons for  $\delta = 0$ ) and may be found by numerical simulation. Figure 6 shows the simulation results for parameters  $\xi = 5.5$  and  $\varepsilon = 0.03$ , where all cluster states are stable: it depends on the initial conditions which state emerges. (The initial conditions are again chosen to be constant functions in the delay interval  $t \in [-\xi, 0]$ .) Notice that spikes are evenly spaced in the splay state in correspondence to the  $S_3$  permutational symmetry. In the 1:2 state, the phase difference between the pair and the singleton depends on the parameters and generally spikes are not evenly spaced. We remark that there are always two different splay states (distinguished by the order of spikes) and three different 1:2 states (distinguished by which oscillator is the singleton). For more details on clustering in globally coupled neural systems, see Brown *et al.* (2003), Coombes (2008) and Orosz *et al.* (2009b).

The different cluster states correspond to periodic orbits in state space and one needs to use Floquet theory to determine their stability. In particular, the eigenvalues of the solution operator of equation (3.1) at  $T_p$ , the so-called Floquet multipliers, need to be calculated. A periodic motion is stable if all the infinitely many multipliers are located inside the unit circle in the complex plane. When varying the parameters, stability losses may occur via fold bifurcation (when a real multiplier crosses the unit circle at +1), via period-doubling bifurcation (when a real multiplier crosses the unit circle at -1) and via Neimark–Sacker bifurcation (when a pair of complex conjugate multipliers crosses the unit circle). Different periodic and quasi-periodic oscillations may arise through these bifurcations that are not discussed here in detail.

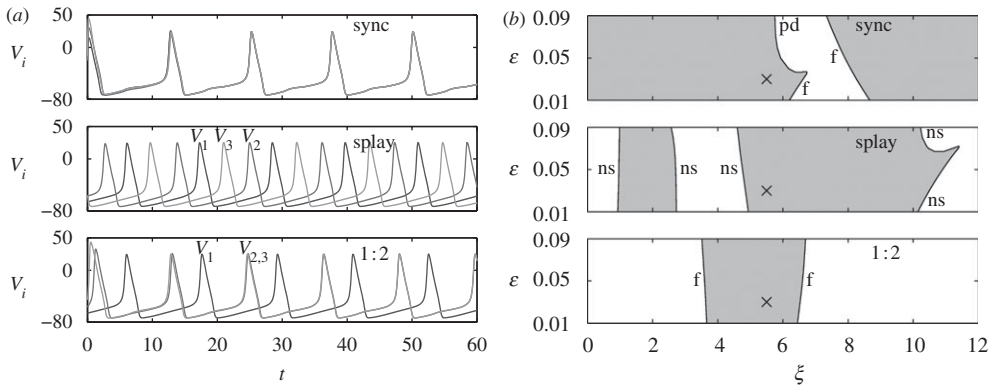


Figure 6. Different neural clusterings are shown in (a) and the related  $(\xi, \varepsilon)$  stability charts are displayed in (b). The shaded domains indicate stability and f, pd and ns denote fold, period doubling and Neimark–Sacker bifurcations. The crosses at  $\xi = 5.5$  and  $\varepsilon = 0.03$  in (b) correspond to the parameters used in (a).

It is not possible to determine the stability boundaries in parameter space analytically but there exist numerical methods to perform this task. We use numerical continuation techniques, in particular the package DDE-BIFTOOL, that allow us to follow branches of oscillatory solutions (both stable and unstable) as a function of parameters and detect the above bifurcations (Roose & Szalai 2007). To determine the stability, the solution operator is discretized and represented by a large matrix whose eigenvalues approximate the Floquet multipliers. We remark that, for large numbers of neurons, one may apply semi-analytical methods to determine the stability for specific cluster states, e.g. the synchronized state and the splay state; see Coombes (2008).

We varied the delay parameter  $\xi$  and detected the above bifurcations for several different values of  $\varepsilon$ ; the results are shown in the stability charts in figure 6b. Shading indicates stability, and the fold, period doubling and Neimark–Sacker bifurcations are denoted by f, pd and ns, respectively. The crosses correspond to the parameter values  $\xi = 5.5$  and  $\varepsilon = 0.03$  used in figure 6a. The ‘sharp edges’ along the stability boundaries correspond to co-dimension-2 bifurcations, e.g. the synchronized state undergoes a fold–period doubling bifurcation and the splay state undergoes a double Neimark–Sacker bifurcation. The dynamics are potentially complex around such points. Furthermore, in certain regimes, multiple unstable solutions coexist with the stable solutions, and the stable manifolds of the unstable solutions separate the regions of attraction of the stable solutions in state space. Unfolding these complexities is beyond the scope of this paper.

By studying the stability diagrams, one may observe qualitative changes of the dynamics as the time delay increases. For small delays (including zero delay), only the synchronous state is stable. This is followed by different domains of mono-, bi- and tristability. That is, by varying the time delay, different cluster states may be realized.

Indeed, it is not possible to tune the natural delays in the system. However, the controller may inject external signals that mimic the effects of delayed coupling. To this end, we construct an event-based act-and-wait controller (Insperger 2006;

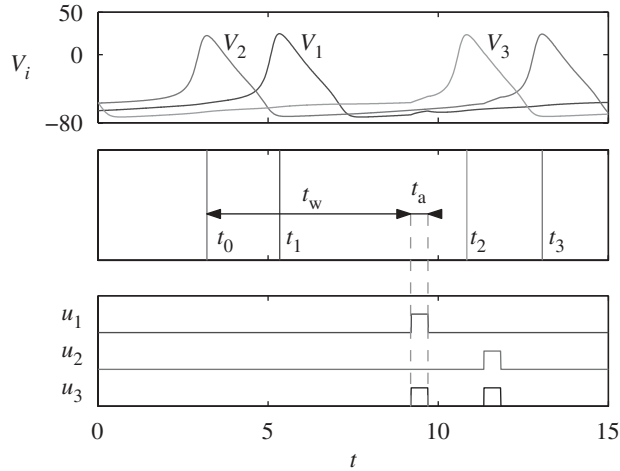


Figure 7. The event-based act-and-wait control algorithm: after a neuron spikes, the controller ‘waits’  $t_w$  time and then ‘acts’ for  $t_a$  time by injecting constant inputs to the other two neurons (see equation (3.2)). Notice that  $t_a \ll t_w$ . From top to bottom: the voltage oscillations, the recorded spike times, the input signals.

Danzl & Moehlis 2007) as follows. We record the event when a neuron spikes (its voltage reaches a local maximum) and, after time  $t_w$ , a constant signal of length  $t_a$  is injected to the other two neurons. The time intervals  $t_w$  and  $t_a$  are called the ‘wait time’ and the ‘act time’, respectively. Considering the initial condition  $u_i(0) = 0, i = 1, 2, 3$ , the control rules can be formalized as follows.

$$\left. \begin{aligned}
 &\text{If neuron } i \text{ spikes at } t = t_0 \text{ then} \\
 &u_j^+(t_0 + t_w) = u_j^-(t_0 + t_w) + 1, \\
 &u_j^+(t_0 + t_w + t_a) = u_j^-(t_0 + t_w + t_a) - 1, \\
 &\text{for all } j \neq i.
 \end{aligned} \right\} \tag{3.2}$$

This algorithm is demonstrated in figure 7. Recall that  $u_i(t)$  can take only the discrete values 0, 1 and 2, where  $u_i(t) = 2$  occurs if at least two neurons spiked within a time interval of  $t_a$ . To obtain ‘spiky’ inputs, we consider  $t_a \ll t_w$ . In particular, we fix the act time at  $t_a = 0.5$  and vary the wait time  $t_w$ .

We define a scalar observable, called the order parameter, to quantify the emergent state of the system,

$$R = \frac{1}{3} | e^{i2\pi(t_1 - t_0)/(t_3 - t_0)} + e^{i2\pi(t_2 - t_0)/(t_3 - t_0)} + e^{i2\pi} |. \tag{3.3}$$

This represents the phase relation of the last four spikes that arrived at  $t_0 \leq t_1 \leq t_2 \leq t_3$ , such that the spikes at  $t_0$  and  $t_3$  were produced by the same neuron, while the spikes at  $t_1$  and  $t_2$  were produced by the other two neurons (see figure 7). This quantity has to be updated when a new spike arrives at  $t_4$  according to the update rule  $t_0 \leftarrow t_1, t_1 \leftarrow t_2, t_2 \leftarrow t_3$  and  $t_3 \leftarrow t_4$ . In fact,  $R$  is an ‘event-based

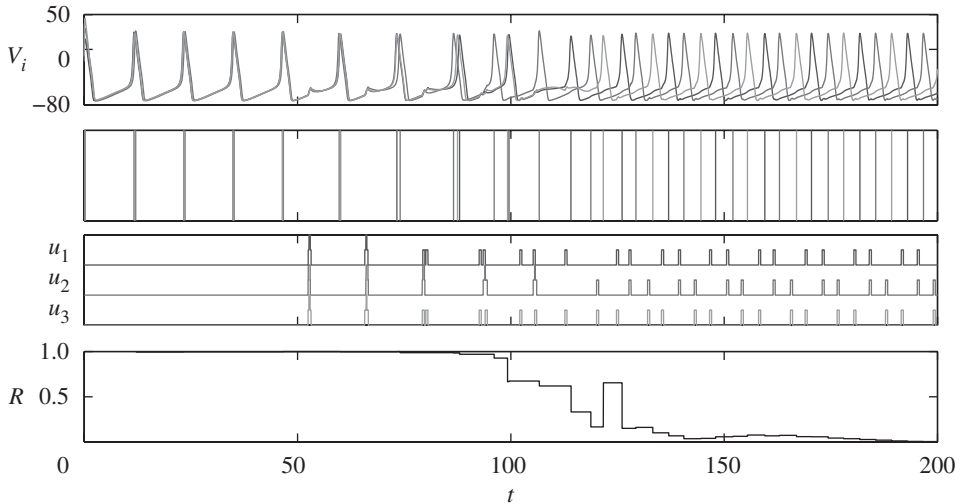


Figure 8. Driving the system from full synchrony to a splay state with the controller for  $\xi = 0$ ,  $\varepsilon = 0.06$  and  $t_w = 6$ . From top to bottom: the voltage oscillations, the recorded spike times, the input signals, the order parameter (3.3).

version' of the order parameter used in phase oscillator networks where the phase information is continuously available (Strogatz 2000). Notice that  $R = 1$  for the fully synchronous state and  $R = 0$  for the splay state (with evenly spaced spikes). For the 1:2 state (with general phase difference between the singleton and the pair), we have  $1/3 \leq R < 1$ ; here, the minimum  $R = 1/3$  is reached when the spikes are evenly spaced.

In figure 8, the controller's action is shown for parameters  $\xi = 0$  and  $\varepsilon = 0.06$ . One may observe that, without inputs ( $t \lesssim 50$ ), the system approaches the fully synchronous state since that is the only stable state for these parameters (see figure 6b). After each neuron has spiked five times, the controller is switched on using  $t_w = 6$ . (Notice that, for  $\xi = 6$  and  $\varepsilon = 0.06$ , the synchronous state is unstable in figure 6b). The controller drives the system away from the fully synchronous state into a splay state as shown in the top two panels in figure 8. The changes in the spatiotemporal pattern of inputs and the time evolution of the order parameter  $R$  (which goes from 1 to 0) are displayed in the bottom panels.

To test the robustness of the proposed algorithm, we vary the wait time  $t_w$  and the coupling strength  $\varepsilon$  (for zero coupling delay  $\xi = 0$ ) and read the asymptotic value of the order parameter (taken at  $t = 1000$ ). The shading of the  $(t_w, \varepsilon)$ -plane in figure 9 represents the value of  $R$  such that white corresponds to  $R = 0$  (splay state), while the darkest tone corresponds to  $R = 1$  (synchronized state). Notice the well-pronounced boundaries between regions of qualitatively different behaviours. We remark that for the 1:2 state we have  $R \approx 1/3$ , meaning that spikes are almost evenly spaced. In the splay\* regime, a splay-like state emerges for which the spikes are not evenly spaced. Such a state may exist since the inputs destroy the  $S_3$  permutation symmetry for  $\delta > 0$ . In the splay\* state, the order

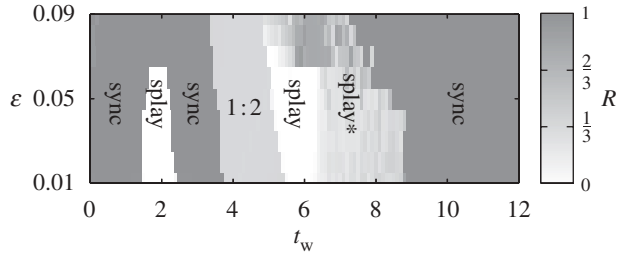


Figure 9. The asymptotic value of the order parameter  $R$  is depicted by shading in the  $(t_w, \varepsilon)$ -plane for  $\xi = 0$ ; see the shading bar on the right. The states approached are written in each regime. The splay\* state is a splay-like state where the spikes are not evenly spaced.

parameter does not approach a particular value but keeps oscillating, resulting in the ‘granular’ shading in this regime. The good match between the location of certain patterns in figures 6*b* and 9 justifies the idea of the controller: the waiting time  $t_w$  can serve as an effective time delay.

Notice that, for larger values of  $\varepsilon$ , the splay regimes become smaller, which may be compensated by slightly increasing the input magnitude  $\delta$ . Choosing different initial conditions in the bi- and tristable regimes in figure 6*b* the emergent states may differ from those in figure 9. For example, for certain initial conditions the synchrony may not be destroyed for  $t_w \approx 2$ , but it always disappears for  $t_w \approx 6$ .

#### 4. Conclusion

In this paper, we demonstrated that designing time delays is an efficient tool for controlling the behaviour of complex biological networks. By varying the delays, one may ‘set the timing’ of the control signals and so stabilize unstable equilibria or unstable oscillations. Thus, one may succeed with the control design even when strong constraints are imposed on the gains and on the qualitative features of the input (which would impede stabilization for zero delay). We demonstrated this strategy in a gene regulatory network and in a neural network by driving the systems away from potentially harmful oscillatory behaviour either to an equilibrium or to a chosen rhythmic cluster state. We achieved this by applying biocompatible inputs.

The considered networks were extremely simple since these were chosen to serve as demonstrative examples. It will be necessary to repeat the calculations for more realistic set-ups (e.g. larger networks) to test the robustness of the proposed algorithms. Ultimately, the controllers also need to be validated by experiments. Nevertheless, we firmly believe that the methodology presented in this paper can be applied to a wide range of biological systems where delays, instead of causing undesired oscillations, can stabilize desired states.

This research was sponsored by the National Science Foundation under grant NSF-0547606 and by the Institute for Collaborative Biotechnologies under grant DAAD19-03-D004 from the US Army Research Office.

## Appendix A. Parameters for the Hodgkin–Huxley model

Here we define the parameters

$$\left. \begin{aligned} g_{\text{Na}} &= 120 \text{ mS cm}^{-2}, & V_{\text{Na}} &= 50 \text{ mV}, \\ g_{\text{K}} &= 36 \text{ mS cm}^{-2}, & V_{\text{K}} &= -77 \text{ mV}, \\ g_{\text{L}} &= 0.3 \text{ mS cm}^{-2}, & V_{\text{L}} &= -54.4 \text{ mV}, \\ \text{and} & & I &= 20 \mu\text{A cm}^{-2}, & C &= 1 \mu\text{F cm}^{-2}, \end{aligned} \right\} \quad (\text{A } 1)$$

and the functions

$$\left. \begin{aligned} \alpha_m(V) &= \frac{0.1(V+40)}{1 - e^{-(V+40)/10}}, & \beta_m(V) &= 4e^{-(V+65)/18}, \\ \alpha_h(V) &= 0.07e^{-(V+65)/20}, & \beta_h(V) &= \frac{1}{1 + e^{-(V+35)/10}}, \\ \alpha_n(V) &= \frac{0.01(V+55)}{1 - e^{-(V+55)/10}}, & \beta_n(V) &= 0.125e^{-(V+65)/80}, \end{aligned} \right\} \quad (\text{A } 2)$$

used in the Hodgkin–Huxley model (3.1).

## References

- Åström, K. J. & Murray, R. M. 2008 *Feedback systems: an introduction for scientists and engineers*. Princeton, NJ: Princeton University Press.
- Bolouri, H. 2008 *Computational modeling of gene regulatory networks—a primer*. London, UK: Imperial College Press.
- Brown, E., Holmes, P. & Moehlis, J. 2003 Globally coupled oscillator networks. In *Perspectives and problems in nonlinear science: a celebratory volume in honor of Larry Sirovich* (eds E. Kaplan, J. E. Marsden & K. R. Sreenivasan), pp. 183–215. New York, NY: Springer.
- Campbell, S. A. 2007 Time delays in neural systems. In *Handbook of brain connectivity* (eds V. K. Jirsa & A. R. McIntosh), pp. 65–90. New York, NY: Springer.
- Chalfie, M., Tu, Y., Euskirchen, G., Ward, W. W. & Prasher, D. C. 1994 Green fluorescent protein as a marker of gene expression. *Science* **263**, 802–805. (doi:10.1126/science.8303295)
- Chen, L. & Aihara, K. 2002 Stability of genetic regulatory networks with time delay. *IEEE Trans. Circuits Syst. I: Fundam. Theory Appl.* **49**, 602–608. (doi:10.1109/TCSI.2002.1001949)
- Coombes, S. 2008 Neuronal network with gap junctions: a study of piecewise linear planar neuron models. *SIAM J. Appl. Dyn. Syst.* **7**, 1101–1129. (doi:10.1137/070707579)
- Coombes, S. & Laing, C. 2009 Delays in activity-based neural networks. *Phil. Trans. R. Soc. A* **367**, 1117–1129. (doi:10.1098/rsta.2008.0256)
- Courey, A. J. 2008 *Mechanisms in transcriptional regulation*. Malden, MA: Blackwell.
- Cox, R. S., Surette, M. G. & Elowitz, M. B. 2007 Programming gene expression with combinatorial promoters. *Mol. Syst. Biol.* **3**, 1–11. (doi:10.1038/msb4100187)
- Danzl, P. & Moehlis, J. 2007 Event-based feedback control of nonlinear oscillators using phase response curves. In *Proc. 46th IEEE Conf. on Decision and Control, New Orleans, LA, 12–14 December 2007*, pp. 5806–5811. Piscataway, NJ: IEEE.
- Dombovári, Z., Wilson, R. E. & Stépán, G. 2008 Estimates of the bistable region in metal cutting. *Phil. Trans. R. Soc. A* **464**, 3255–3271. (doi:10.1098/rspa.2008.0156)
- Dunlap, J. C. 1999 Molecular bases for circadian clocks. *Cell* **96**, 271–290. (doi:10.1016/S0092-8674(00)80566-8)
- Elowitz, M. B. & Leibler, S. 2000 A synthetic oscillatory network of transcriptional regulators. *Nature* **403**, 335–338. (doi:10.1038/35002125)

- Ermentrout, B. & Ko, T.-W. 2009 Delays and weakly coupled neuronal oscillators. *Phil. Trans. R. Soc. A* **367**, 1097–1115. (doi:10.1098/rsta.2008.0259)
- Gardner, T. S., Cantor, C. R. & Collins, J. J. 2000 Construction of a genetic toggle switch in *Escherichia coli*. *Nature* **403**, 339–342. (doi:10.1038/35002131)
- Hodgkin, A. L. & Huxley, A. F. 1952 A quantitative description of membrane current and its application to conduction and excitation in nerve. *J. Physiol.* **117**, 500–544.
- Inspurger, T. 2006 Act-and-wait concept for continuous-time control systems with feedback delay. *IEEE Trans. Control Syst. Technol.* **14**, 974–977. (doi:10.1109/TCST.2006.876938)
- Kirst, C., Geisel, T. & Timme, M. 2009 Sequential desynchronization in networks of spiking neurons. *Phys. Rev. Lett.* **102**, 068101. (doi:10.1103/PhysRevLett.102.068101)
- Mascolo, S. 1999 Congestion control in high-speed communication networks using the Smith principle. *Automatica* **35**, 1921–1935. (doi:10.1016/S0005-1098(99)00128-4)
- Monk, N. A. M. 2003 Oscillatory expression of Hes1, p53, and NF- $\kappa$ B driven by transcriptional time delays. *Current Biol.* **13**, 1409–1413. (doi:10.1016/S0960-9822(03)00494-9)
- Novák, B. & Tyson, J. J. 2008 Design principles of biochemical oscillators. *Nat. Rev. Mol. Cell Biol.* **9**, 981–991. (doi:10.1038/nrm2530)
- Olfati-Saber, R. & Murray, R. M. 2004 Consensus problems in networks of agents with switching topology and time delays. *IEEE Trans. Autom. Control* **49**, 1520–1533. (doi:10.1109/TAC.2004.834113)
- Orosz, G., Ashwin, P. & Townley, S. 2009a Learning of spatio-temporal codes in a coupled oscillator system. *IEEE Trans. Neural Networks* **20**, 1135–1147. (doi:10.1109/TNN.2009.2016658)
- Orosz, G., Moehlis, J. & Ashwin, P. 2009b Designing the dynamics of globally coupled oscillators. *Progr. Theoret. Phys.* **122**, 611–630. (doi:10.1143/PTP.122.611)
- Popovych, O., Hauptmann, C. & Tass, P. A. 2006 Control of neuronal synchrony by nonlinear delayed feedback. *Biol. Cybern.* **95**, 69–85. (doi:10.1007/s00422-006-0066-8)
- Rabinovich, M. I., Varona, P., Selverston, A. I. & Abarbanel, H. D. I. 2006 Dynamical principles in neuroscience. *Rev. Mod. Phys.* **78**, 1213–1265. (doi:10.1103/RevModPhys.78.1213)
- Roose, D. & Szalai, R. 2007 Continuation and bifurcation analysis of delay differential equations. In *Numerical continuation methods for dynamical systems* (eds B. Krauskopf, H. M. Osinga & J. Galan-Vioque), pp. 359–399. New York, NY: Springer.
- Sarpeshkar, R., Wattanapanitch, W., Arfin, S. K., Rapoport, B. I., Mandal, S., Baker, M. W., Fee, M. S., Musallam, S. & Andersen, R. A. 2008 Low-power circuits for brain–machine interfaces. *IEEE Trans. Biomed. Circuits Syst.* **2**, 173–183. (doi:10.1109/TBCAS.2008.2003198)
- Stépán, G. 1989 Retarded dynamical systems: stability and characteristic functions. In *Pitman research notes in mathematics*, vol. 210. Harlow, UK: Longman.
- Stépán, G. 2001 Vibrations of machines subjected to digital force control. *Int. J. Solids Struct.* **38**, 2149–2159. (doi:10.1016/S0020-7683(00)00158-X)
- Stricker, J., Cookson, S., Bennett, M. R., Mather, W. H., Tsimring, L. S. & Hasty, J. 2008 A fast, robust and tunable synthetic gene oscillator. *Nature* **456**, 516–519. (doi:10.1038/nature07389)
- Strogatz, S. H. 2000 From Kuramoto to Crawford: exploring the onset of synchronization in populations of coupled oscillators. *Physica D* **143**, 1–20. (doi:10.1016/S0167-2789(00)00094-4)
- Ugander, J. 2008 Delay-dependent stability of genetic regulatory networks. Master’s thesis, Department of Automatic Control, Lund University, Sweden. <https://www.control.lth.se/database/publications/article.pike?artkey=5819>.